Solvent Effects on Interfacial Electron Transfer from Ru(4,4′-dicarboxylic acid-2,2′-bipyridine)$_2$(NCS)$_2$ to Nanoparticulate TiO_2: Spectroscopy and Solar Photoconversion†

Jennifer A. Pollard, Dongshe Zhang, Jonathan A. Downing, Fritz J. Knorr, and Jeanne L. McHale*

Department of Chemistry, Washington State University, Box 99164-4630, Pullman, Washington 99164-4630

Received: June 30, 2005; In Final Form: September 28, 2005

Resonance Raman spectra are reported for Ru(4,4′-dicarboxylic acid-2,2′-bipyridine)$_2$(NCS)$_2$ (commonly called "N3") in ethanol solution and adsorbed on nanoparticulate colloidal TiO_2 in ethanol (EtOH) and in acetonitrile (ACN), at wavelengths within the visible absorption band of the dye. Raman cross sections of free N3 in EtOH are found to be similar to those of N3 adsorbed on colloidal TiO_2 in EtOH, and are generally lower than those of N3 on TiO_2 in ACN. Strong electronic coupling mediated by surface states results in red-shifted absorption spectra and enhanced Raman signals for N3 adsorbed on nanocolloidal TiO_2 in ACN compared to EtOH. In contrast, the absorption spectrum of N3 on nanocrystalline TiO_2 in contact with solvent is similar for ACN and EtOH. Wavelength-dependent depolarization ratios for N3 Raman bands of both free and adsorbed N3 reveal resonance enhancement via two or more excited electronic states. Luminescence spectra of N3 adsorbed on nanocrystalline films of TiO_2 and ZrO_2 in contact with solvent reveal that the quantum yield of electron injection ϕ_{ET} into TiO_2 decreases in the order ACN > EtOH > DMSO. Dye-sensitized solar cells were fabricated with N3 adsorbed on nanocrystalline films of TiO_2 in contact with ACN, EtOH, and DMSO solutions containing LiI/LiI_3 electrolyte. Photoconversion efficiencies η were found to be 2.6% in ACN, 1.3% in DMSO, and 0.84% in EtOH. Higher short circuit currents are found in cells using ACN, while the maximum voltage is found to be largest in DMSO. It is concluded that the increased photocurrent and quantum yield of interfacial electron transfer in acetonitrile as compared to ethanol and DMSO is primarily the result of faster electron injection of N3 when adsorbed on TiO_2 in the presence of ACN as opposed to EtOH or DMSO.

1. Introduction

Dye-sensitized solar cells (DSSCs) are photovoltaic devices which use light harvesting dyes (sensitizers) adsorbed on nanoparticles of wide-band gap semiconductors such as TiO_2 for the conversion of light to electricity.[1−4] One of the most efficient sensitizers to date is Ru(4,4′-dicarboxylic acid-2,2′-bipyridine)$_2$(NCS)$_2$, also called N3 (Figure 1), for which energy conversion efficiencies as high as 10% have been reported.[5] The semiconductor is typically nanocrystalline TiO_2 in the form of anatase, with particle sizes of about 15 nm, affording high surface area for optimal light harvesting by a monolayer of adsorbed dye. The anode in the DSSC consists of porous nanocrystalline TiO_2 deposited as a thin film on a transparent conductive electrode (TCE) and sensitized with a monolayer of light harvesting dye (D) in contact with a liquid solution containing a redox couple, typically I^-/I_3^-. The cell is completed by a counter electrode consisting of Pt-coated TCE. Following excitation by visible photons, the excited state of the dye is thermodynamically poised to inject electrons into TiO_2, resulting in oxidation of the dye and producing conduction band electrons, which then move through the external circuit to the counter electrode, where they are captured by I_3^-. The reduced form of the sensitizer is regenerated by reaction with I^-, completing the cycle. A crucial factor in the overall energy conversion efficiency is the quantum yield ϕ_{ET} for the primary step of interfacial electron transfer (ET) from excited sensitizer D* to TiO_2, which for N3 is near unity at wavelengths within its visible absorption spectrum.[5] From time-resolved spectroscopy measurements, a large share of this interfacial ET has been found to take place on a subpicosecond time scale, implicating ET from vibrationally excited states.[6−16] Though a high quantum yield ϕ_{ET} requires that ET be sufficiently fast to compete with energy-wasting radiative and nonradiative relaxation of D*, it has been pointed out[16] that ultrafast ET is not necessarily

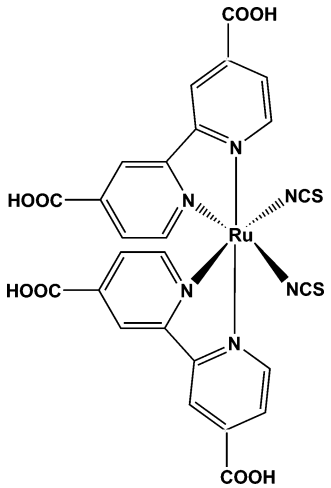

Figure 1. Structure of N3.

† Part of the special issue "Jack Simons Festschrift".

10.1021/jp053595z CCC: $30.25
Published on Web 11/15/2005

beneficial to the DSSC owing to the concomitant increase in the rate of reverse ET, in which conduction band electrons recombine with oxidized dye.

The energy conversion efficiency of the DSSC has been optimized with respect to many factors, including the nature of the electrolyte solution. Efficiencies can be further improved by the use of additives such as *tert*-butylpyridine which hinder recombination of conduction band electrons with oxidized dye or I_3^-, increasing the photovoltage,[17] and by the addition of potential determining ions such as Li^+ which result in anodic shifts of the conduction band.[18] Despite intensive efforts to better understand the microscopic basis for the performance of the DSSC (see for example the July 2004 issue of *Coordination Chemistry Reviews*), the influence of the solvent on the quantum yield for interfacial electron transfer (ET) and the overall energy conversion efficiency has not been widely considered. N3 photodegrades slowly in the presence of water, and several different nonaqueous solvents have been employed in the DSSC, notably acetonitrile, binary mixtures of acetonitrile with 3-methyl-2-oxazolidinone,[5] 3-methoxypropionitrile,[19] or propylene carbonate.[20] Acetonitrile is frequently used as a solvent for electrochemistry as a result of its relatively low viscosity, high dielectric constant, and resistance to oxidation.[21] Meyer et al. studied the effect of solvent on incident photon-to-current conversion efficiencies in a DSSC sensitized with a Ru-based coordination compound and found large variations attributed to solvent effects on the collection efficiency for injected electrons in the external circuit.[22] In the present work, we consider the potential of the solvent to influence the quantum yield of the initial electron injection as well as the overall efficiency for conversion of light to electricity.

The subpicosecond electron injection of N3 on TiO_2 nanocrystalline films is followed by slower relaxation that has been variously attributed to injection from vibrationally relaxed states within the triplet excited state manifold, or to injection from dye aggregates.[14] Sundström et al.[7] measured the picosecond kinetics of electron injection in N3/TiO_2 in contact with EtOH and ACN by following the transient absorption of the oxidized dye and found generally slower ET in EtOH than in ACN, manifested by a smaller amplitude of the fastest component and longer time scale for the slowest component of the transient spectrum. McCusker et al.[13] found the fastest component of ET kinetics to be independent of solvent while the amplitude of a component at ~11 ps decreased on going from ACN to EtOH, and was smaller still for a dry film. In another study, Durrant et al.[15] found the subpicosecond kinetics of ET from N3 to TiO_2 to be the same whether the film was in contact with air or organic solvent. The dynamics of the free dye have also been studied as a function of solvent and found to differ in acetonitrile, ethanol, and methanol, an effect that was attributed to solvent effects on interligand electron transfer in excited state relaxation.[23] Interligand electron transfer was also concluded to play a role in triplet state ET from N3 to TiO_2.[7]

Solvent effects can enter into the picture for the DSSC in a number of ways, by influencing (1) the energy of the TiO_2 conduction band (E_{CB})[24] and/or that of the dye excited state redox potential, (2) the solvent contribution to the reorganization energy for ET, (3) the electronic coupling of sensitizer and semiconductor, (4) the rate of nonradiative relaxation of the dye excited state, (5) the redox potential of the I^-/I_3^- couple,[25] and (6) the rate at which the reduced form of N3 is regenerated by reaction of $N3^+$ with I^-. While the overall efficiency of solar energy conversion could be affected by any of these factors, the first three determine the rate of ET and along with (4) influence the quantum efficiency ϕ_{ET}.

Resonance Raman spectroscopy is employed here to investigate the influence of the solvent on ultrafast ET from the excited electronic state of N3 to TiO_2 in transparent nanocolloidal suspensions in ethanol (EtOH) and acetonitrile (ACN). We have previously demonstrated the utility of resonance Raman spectroscopy for the study of dynamics of excited electronic states.[26] In this work we sought to observe the influence of interfacial ET on the N3 Raman cross sections. Absolute Raman intensities determined by reference to a solvent Raman band have been employed by our lab[26] and others[27] to determine solvent and internal reorganization energies of charge-transfer electronic transitions using time-dependent theory.[28] Colloidal suspensions of TiO_2 nanoparticles, as opposed to nanocrystalline films, are advantageous in the present work as they are easily stirred or circulated to prevent photodecomposition during Raman measurements, and N3 Raman cross sections can be determined from the known concentrations of solvent and sensitizer. We report Raman excitation profiles of N3 vibrational modes at a range of visible wavelengths for N3 in EtOH and N3 adsorbed on TiO_2 in both EtOH and ACN. (The free dye is insoluble in ACN.) In the time-dependent view of resonance Raman spectroscopy,[28] solvent relaxation and excited state decay limit the intensity of the Raman signals, while increasing internal reorganization correlates with enhanced Raman intensity. Thus excited state ET occurring on the Raman time scale could conceivably result in lower Raman intensities for N3/TiO_2 compared to N3 in solution, all other factors being equal.

The Loppnow group previously determined resonance Raman excitation profiles for N3 in dimethyl sulfoxide (DMSO) and N3 adsorbed on colloidal TiO_2 in DMSO.[29] They actually found somewhat larger Raman intensities for the adsorbed dye despite a decrease in internal reorganization energy, a result of the overriding influence of smaller solvent reorganization energy compared to the free dye in solution. Their analysis took into account the putative ^{1}MLCT transition associated with the ~540 nm absorption maximum, and a lower lying transition to the red of this band attributed to a transition to a triplet (^{3}MLCT) excited state. The two main peaks in the visible absorption spectrum of N3 at ~ 400 and 540 nm are often attributed to transitions to two different ^{1}MLCT excited states, while a sharp band at about 320 nm has been assigned to a ligand-based $\pi-\pi^*$ transition.[30] However, recent quantum calculations on N3 have concluded that transitions to numerous closely spaced, low oscillator strength MLCT transitions add to give the observed visible spectrum.[31,32] These calculations are supported to some extent by results presented in ref 33, where the excited state relaxation of N3 in ethanol following 410 nm excitation was concluded to take place via a multitude of singlet excited states. In the present work, Raman depolarization ratios as well as excitation profiles are determined as a function of wavelength to address the possibility of multiple resonant electronic states of N3. Depolarization ratios are found to deviate considerably from the value of 1/3 expected for resonance with a single nondegenerate electronic state. Unfortunately, the existence of multiple resonant electronic states renders the application of time-dependent theory impracticable. We do observe increased Raman intensity for N3/TiO_2 in ACN compared to EtOH that appears to correlate with the red-shifted absorption spectrum of the former.

Though colloidal nanoparticles of TiO_2 are convenient for spectroscopic measurements, the particles as initially obtained

from hydrolysis of titanium halides or alkoxides are typically amorphous and have a high concentration of defect states which can mediate interfacial electron transfer, particularly recombination dynamics.[34−36] Owing to the larger surface-to-volume ratio in nanoparticles compared to bulk semiconductors, surface trap states such as Ti(III) centers associated with oxygen vacancies can be extremely important. In functioning DSSCs, TiO_2 is prepared as a thin film of nanocrystalline (anatase) particles by sintering in air at temperatures above 400 °C. Though these nanocrystalline films are thought to contain fewer trap states than amorphous nanoparticles, surface defects are still present and there is great interest in surface modification strategies for improving the efficiency of the DSSC.[19,37] Resonance Raman spectra of dyes adsorbed on thin films of nanocrystalline TiO_2 have been reported,[38,39] but are problematic for the determination of absolute intensities. (The relative concentration of dye and solvent in the sampled volume is unknown in the case of a thin film in contact with solvent.) In this work, we compare luminescence and absorption spectra of N3 on colloidal (amorphous) TiO_2 and on nanocrystalline TiO_2 films in contact with solvent, in order to determine the influence of solvent and nanoparticle crystallinity on ϕ_{ET}. DSSCs were prepared using N3-sensitized nanocrystalline films of TiO_2 on F:SnO_2 TCE in contact with electrolyte solutions containing LiI and LiI_3 in ACN, EtOH, and DMSO, and photocurrent/photovoltage data are reported for visible light illumination. The luminescence and photocurrent/photovoltage data reveal strong solvent effects on the efficiency of interfacial electron transfer and solar energy conversion. Results are interpreted in terms of solvent effects on the rate of interfacial electron transfer and recombination dynamics.

2. Experimental Section

Colloidal TiO_2. Colloidal suspensions of TiO_2 nanoparticles for spectroscopy were synthesized by solvolysis of $TiCl_4$ in ethanol at 1 °C following the procedure of ref 40 to give a final concentration of 10 mM TiO_2. At this temperature the resulting average particle size is reported to be on the order of 6 nm. Raman spectroscopy of the transparent colloidal suspensions did not show evidence of the strong Raman line of anatase at 144 cm^{-1},[41,42] consistent with the formation of amorphous TiO_2,[43] though weak Raman lines of rutile at about 450 and 610 cm^{-1} [42] were present. Nanoparticles prepared in ethanol solution were dried under vacuum and redispersed in dry acetonitrile. TiO_2 suspensions in ethanol were found to be stable for many months, but those in acetonitrile were prone to aggregation and precipitation over time, though this problem could be inhibited somewhat by rigorous exclusion of water. Negligible changes in the absorption spectrum of sensitized nanoparticles were observed following measurement of the Raman spectrum, confirming sample integrity. N3 was purchased from Solaronix and used as received. For Raman measurements, a solution of N3 in dry ethanol was added to the TiO_2 suspension and stirred overnight to form a final concentration of 10 mM TiO_2 and 0.227 mM N3. This solution was then dried on a vacuum line, and the sensitized nanoparticles were redispersed in dry acetonitrile. Solutions of sensitized nanoparticles were assumed to contain negligible amounts of free N3 based on the observation of colorless supernatant upon precipitation. In addition, sensitized nanocrystalline thin films, described below, can be stored in neat ACN or EtOH with negligible loss of N3.

Luminescence spectra of colloidal nanoparticles were obtained using a QuantaMaster QM4 fluorimeter from Photon Technology Inc. Absorption spectra were obtained using a Shimadzu UV-2501 spectrometer. Raman measurements were performed in a magnetically stirred, sealed quartz cuvette using excitation from either an argon ion laser (Coherent Innova 400), a krypton ion laser (Spectra Physics Beamlock 2060), or a ring dye laser (Coherent 800) pumped by the argon ion laser. The excitation light was focused onto the sample with a cylindrical lens, and the backscattered light was focused into the entrance slit of a single monochromator (Acton Spectro-Pro 2300i) after passing through a holographic notch filter (Kaiser Optical) to remove the elastically scattered light. The laser power at the sample was typically about 80 mW, and the scattered light was detected using a thermoelectrically cooled CCD (Roper Scientific, Spec10:256E). Polarized and depolarized Raman spectra were corrected for self-absorption and for the wavelength-dependent instrument response measured using a quartz-halogen standard lamp (Oriel). Representative Raman spectra of a few samples (see Figure 6) were also recorded at higher resolution using a scanning double monochromator with photomultiplier tube detection. Raman intensities of N3 and solvent lines were based on areas of peaks which were fit to Lorentzian functions. Absolute Raman cross sections of the solvent standards (918 cm^{-1} for ACN and 880 cm^{-1} for EtOH) were taken from ref 44 and ref 45, respectively.

The total cross section σ_R for a particular mode at a given wavelength is related to the differential cross section as follows:

$$\sigma_R = \frac{8\pi}{3}\frac{(1+2\rho)}{(1+\rho)}\frac{d\sigma}{d\Omega} \tag{1}$$

where the differential cross section $d\sigma/d\Omega$ is the sum of the contributions for parallel and perpendicular scattering, and ρ is the depolarization ratio. The relative intensities of two Raman bands are dependent on the concentrations C_1 and C_2 of the two components and their differential cross sections as follows:

$$\frac{I_1}{I_2} = \frac{C_1}{C_2}\frac{d\sigma_1/d\Omega}{d\sigma_2/d\Omega} \tag{2}$$

enabling the differential and then the total cross section of N3 bands to be determined from the known Raman cross sections of the solvent standards. The reported total cross sections have an estimated uncertainty of ±15%. Depolarization ratios are reported as $\rho = I_{VH}/I_{VV}$, where the incident light is vertically polarized in either case, and I_{VH} (I_{VV}) is the intensity of scattered light with polarization perpendicular (parallel) to that of the incident beam, corrected for instrument response. The estimated uncertainty in the reported depolarization ratios is less than ±0.05.

Nanocrystalline TiO_2. Thin films of nanocrystalline TiO_2 (Degussa P25, nominal 25 nm particle size) on F:SnO_2 (Hartford Glass) were prepared following the method of ref 5 and ref 46 and reveal Raman scattering peaks assigned to anatase. Sensitized films were prepared by soaking in ethanolic solution of N3 overnight. These nanocrystalline films were used for luminescence measurements and for the electrode in the DSSC as described further below. Thin films of ZrO_2 (Aldrich, particle size 20−30 nm) on conductive glass for luminescence spectra were prepared and sensitized following the same approach as for TiO_2. Absorption spectra of transparent nanocrystalline films of TiO_2 were obtained using TiO_2 purchased from Solaronix (nominal 9 nm particle size), deposited on glass cover slips and heated at 450 °C for 30 min. Spectra were recorded for films in contact with air or solvent and covered with a second cover slip.

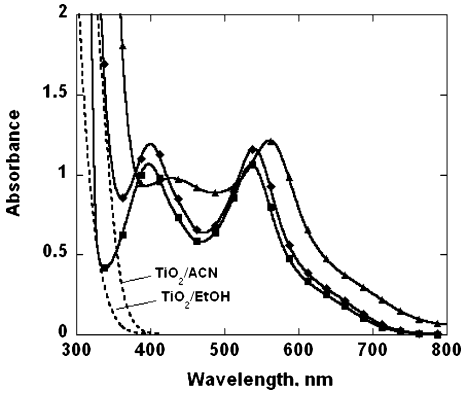

Figure 2. Absorption spectra of 0.091 mM N3 (solid lines) in EtOH (squares), in 4.0 mM colloidal TiO_2/EtOH (diamonds), and in 4.0 mM colloidal TiO_2/ACN (triangles) and absorption spectra of 1.0 mM colloidal TiO_2 (dashed lines) in EtOH and in ACN. The reference in all spectra is the neat solvent.

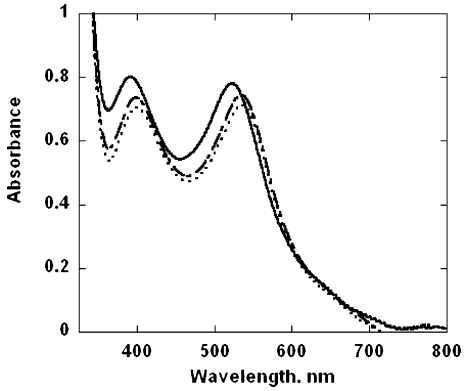

Figure 3. Absorption spectrum of N3-sensitized nanocrystalline film of TiO_2 on glass in contact with air (solid line), EtOH (dashed line), and ACN (dotted line). The reference was the same TiO_2 film on glass without N3, in contact with air or solvent.

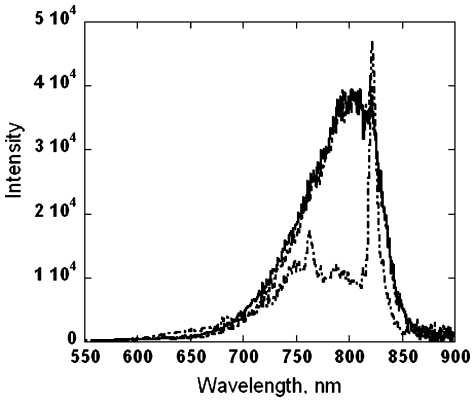

Figure 4. Emission spectrum of 0.227 mM N3 excited at 530 nm in EtOH (solid line), in 10 mM colloidal TiO_2 in EtOH (dashed line), and in 10 mM colloidal TiO_2 in ACN (dot−dashed line). The sharp features in the last spectrum are scattering artifacts of the excitation beam, as determined from experiments with long pass filters.

Luminescence spectra of the sensitized nanocrystalline films in 1 cm quartz cuvettes containing solvent were excited with 10 mW of light at 530.9 nm, using the same instrumentation as was employed for the Raman spectra. Solar cells were fabricated by preparing 10 μm films of TiO_2 (Degussa P25) on F-doped SnO_2 (Hartford Glass) following the procedures of refs 5 and 46. These films were heated to 450 °C for 30 min in air, immersed in ethanolic N3 solution while still warm, and left to soak overnight. The sensitized films were cut into sections for comparison in different solvents. The counter electrode consisted of Pt-coated F:SnO_2, and the electrolyte solution consisted of 0.5 M LiI and 0.05 M I_2 in dry acetonitrile (ACN), ethanol (EtOH), or dimethyl sulfoxide (DMSO). The DSSC was illuminated with 100 mW/cm^2 of visible light from a 75 W xenon lamp, using an illuminated area of 0.196 cm^2 and UV and IR filters in front of the sample. Measurements of photocurrent and photovoltage were performed using a Keithley model 2400 SourceMeter, and incident light power was measured with a Melles-Griot bolometer. The surface concentration of the dye for current−voltage measurements, based on the projected rather than actual area of the film, was determined by desorption into a known volume of aqueous NaOH followed immediately by measurement of the absorption spectrum, using a molar absorptivity of 1.18×10^4 M^{-1} cm^{-1} at the absorption maximum of 500 nm.

3. Results

3.1. Absorption and Luminescence. Figure 2 shows the absorption spectrum of N3 in EtOH and on colloidal TiO_2 nanoparticles in ACN and EtOH, along with that of unsensitized colloidal TiO_2 in the same solvents. The absorption spectrum of N3 on TiO_2 in EtOH is very similar to that of the free dye in the same solvent; the molar absorptivity was found to be 12,000 M^{-1} cm^{-1} at 530 nm in both samples, in good agreement with ref 47. By comparison, the absorption spectrum of N3 on colloidal TiO_2 in ACN is broadened, red-shifted, and increased in intensity, having molar absorptivity of 12,300 M^{-1} cm^{-1} at the absorption maximum of 560 nm. The relative intensity of the ~400 nm band compared to the ~530 nm band is diminished for N3-sensitized nanoparticles in ACN as compared to both free and adsorbed N3 in EtOH. N3 is known to be negatively solvatochromic,[47] so based solely on the similar bulk dielectric constants of ACN and EtOH, the red-shift of the spectrum in ACN is unexpected. Shoute and Loppnow[29] also found the relative intensity of the ~400 nm band to be smaller for N3/TiO_2 in DMSO compared to the free dye in DMSO, but no red-shift of the adsorbed dye was reported.

We note also that a consistent red-shift of the band edge of unsensitized colloidal TiO_2 nanoparticles was observed in ACN compared to EtOH, as shown in Figure 2. The absorption spectrum of sintered nanocrystalline TiO_2 films in contact with ACN or EtOH did not depend on solvent (not shown). The absorption spectrum of a sintered nanocrystalline TiO_2 film sensitized with N3 in contact with solvent was similar for ACN and EtOH (Figure 3), though a slight red shift was observed for N3/TiO_2 films in contact with either solvent as opposed to air. We speculate that the observed solvent effects on the band gap absorption of nanocolloidal TiO_2 observed here are the result of surface states which contribute to absorption below the band gap in the case of amorphous TiO_2 in ACN.[48]

Figure 4 compares the luminescence spectrum of free N3 in EtOH to nanocolloidal N3/TiO_2 in ACN and EtOH, all samples excited at 530 nm and containing the same concentration of N3. The emission maximum at about 800 nm, in good agreement with ref 47, is reasonably assigned to a transition from the triplet excited state to the singlet ground state. The luminescence of free N3 in EtOH is indistinguishable from that of N3/TiO_2 in EtOH, indicating negligible quenching due to interfacial ET. The luminescence of N3/TiO_2 in ACN is considerably less than in both the EtOH samples, and the decrease is greater than can be attributed to slight differences in the absorption of the excitation beam and the emitted light.

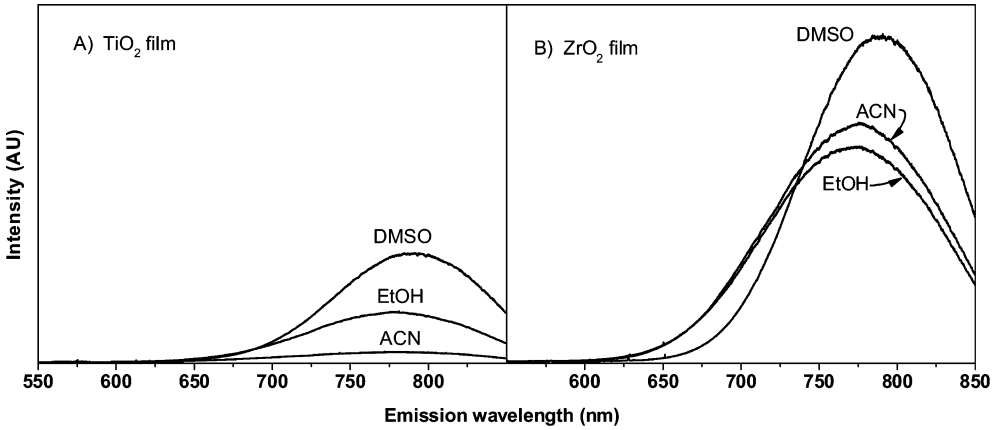

Figure 5. Emission spectrum excited at 530 nm of N3-sensitized nanocrystalline film of TiO_2 (left) and ZrO_2 in contact with ACN, EtOH, and DMSO. All spectra are represented on the same intensity scale after correcting for the difference in dye loading, which was 2.62×10^{-8} mol/cm^2 for ZrO_2 and 8.82×10^{-8} mol/cm^2 for TiO_2.

Luminescence spectra of N3 on nanocrystalline TiO_2 and ZrO_2, in contact with ACN, EtOH, and DMSO, are shown in Figure 5. The same TiO_2 or ZrO_2 film was used in each experiment, and care was taken to change the contacting solvent without disturbing the alignment of the film. Heterogeneity of the films also contributes to small variations in emission intensity for different positions of the sample. From replicate measurements the effect of alignment introduces an error of approximately ±10% in the intensity of the emission. The conduction band of ZrO_2 is about 1 eV higher than that of TiO_2; thus no interfacial ET is expected for N3 on ZrO_2.[49] The luminescence intensity for N3/ZrO_2 decreases in the order DMSO > ACN > EtOH, compared to N3/TiO_2 where the order is DMSO > EtOH ≫ ACN.

The quantum yield of emission provides a means to determine variations in the yield ϕ_{ET} of interfacial ET. In the absence of ET, i.e., for the free dye in solution or adsorbed on ZrO_2, the quantum yield for emission is given by

$$\phi_{em} = \frac{k_{rad}}{k_{rad} + k_{non}} \tag{3}$$

where k_{rad} and k_{non} are the radiative and nonradiative relaxation rates, respectively. In samples containing TiO_2, the emission quantum yield is given by

$$\phi_{em}' = \frac{k_{rad}}{k_{rad} + k_{non} + k_{et}} \tag{4}$$

where k_{et} is the rate of interfacial ET and it is assumed that surface adsorption of the dye does not perturb the radiative and nonradiative relaxation rates. The quantum yield for ET is then found to be

$$\phi_{ET} = \frac{k_{et}}{k_{et} + k_{rad} + k_{non}} = 1 - \frac{\phi_{em}'}{\phi_{em}} \tag{5}$$

The absence of a quenching effect in EtOH for N3 adsorbed on TiO_2 nanoparticles is consistent with the absence of interfacial ET to colloidal nanoparticles in this solvent, as opposed to those in ACN where the luminescence is partially quenched. In the case of N3 adsorbed on a nanocrystalline ZrO_2 film, the relative intensities reflect solvent contributions to nonradiative relaxation which increase on going from DMSO to ACN to EtOH. The nanocrystalline N3/TiO_2 films, on the other hand, reveal the additional effects of the contacting solvent on k_{et}, and the large relative decrease in emission in the case of ACN is evidence for faster interfacial ET in this solvent compared to EtOH and DMSO. Using eq 5, quantum efficiencies ϕ_{ET} for N3 on nanocrystalline TiO_2 were estimated to be about 0.98 in ACN, ∼0.9 in EtOH, and ∼0.8 in DMSO. The incident photon-to-current conversion efficiency for a N3 based DSSC using LiI/LiI_3 electrolyte in ACN has been reported to be ∼85−90% at wavelengths within the lowest lying absorption band,[5] and is consistent with the strong quenching of N3 luminescence reported here for N3-sensitized TiO_2 in contact with ACN.

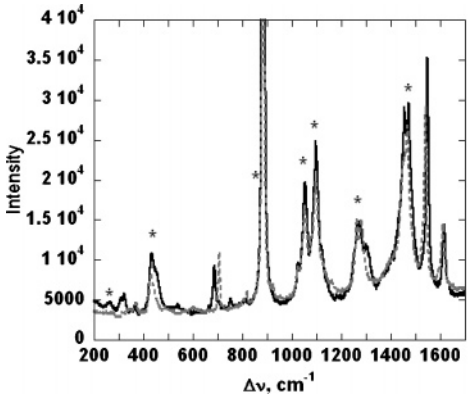

Figure 6. Raman spectrum of 0.227 mM N3 in EtOH (solid line) and in 10 mM TiO_2 (dashed line), excited at 514 nm. The asterisks indicate interference from EtOH Raman bands.

3.2. Resonance Raman Spectra. Representative resonance Raman spectra excited at 514 nm of N3 in EtOH and N3 on colloidal TiO_2 in EtOH are shown in Figure 6, and the Raman spectrum of N3/TiO_2 in ACN excited at 496 nm is shown in Figure 7. A number of N3 Raman bands are obscured by overlapping solvent Raman bands. For the most part there are only slight changes in the Raman frequencies of free versus adsorbed N3, in accordance with weak perturbation to the ground state structure of N3 on adsorption. Exceptions are the 680 cm^{-1} vibration of free N3, assigned to an in-plane bipyridyl ring deformation, which shifts to 705 cm^{-1} in N3/TiO_2 in EtOH and to 700 cm^{-1} in N3/TiO_2 in ACN. Several weak low-frequency modes of the free dye in EtOH are absent for N3 on TiO_2. An in-plane ring deformation at 744 cm^{-1} in the free dye is apparently absent in the adsorbed dye in EtOH, while the mode at 809 cm^{-1} shifts to 816 cm^{-1} on TiO_2 in EtOH. This band is overlapped by a solvent band in the ACN sample. The bipyridine ring stretches at 1548 and 1615 cm^{-1} for N3 in EtOH are both slightly red-shifted, to ∼1540 and ∼1610 cm^{-1},

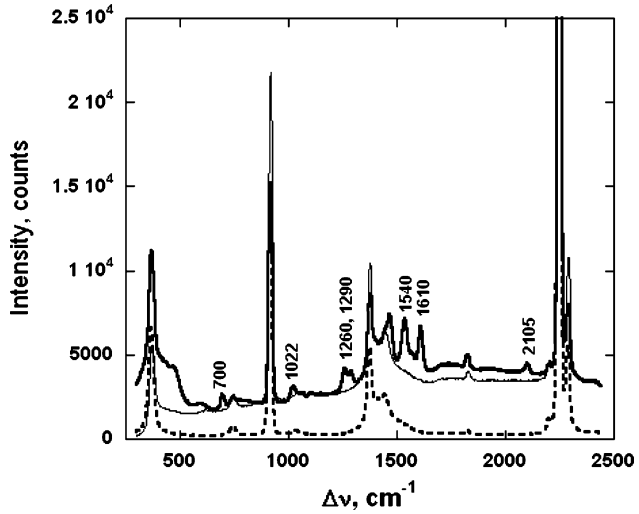

Figure 7. Raman spectrum of ACN (dashed line), of 10 mM TiO_2 in ACN (thin solid line), and of 0.227 mM N3, 10 mM TiO_2 in ACN (thick solid line) excited at 496 nm. The frequencies of the major Raman bands of N3 are labeled.

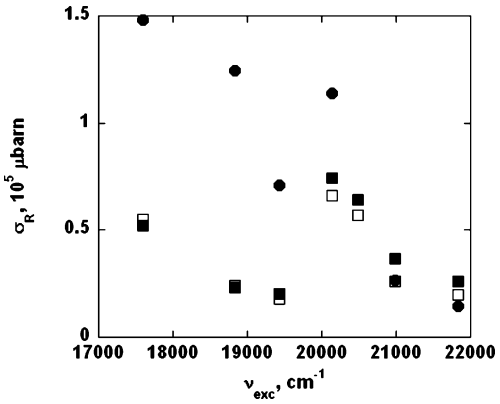

Figure 8. Raman cross section σ_R of the ~700 cm^{-1} Raman band of N3 as a function of excitation wavelength for N3 in EtOH (open squares), on TiO_2 in EtOH (filled squares), and on colloidal TiO_2 in ACN (filled circles).

respectively, in N3/TiO_2 in both solvents. Interestingly, the Loppnow study[29] of N3 and N3/TiO_2 in DMSO found a similar blue-shift in the ~680 cm^{-1} vibration on adsorption, but no effect on the mode at 750 or 1610 cm^{-1}. This raises the question of whether the solvent could influence the way N3 binds to TiO_2. It is interesting that the C≡N stretch which appears at 2118 cm^{-1} in N3/EtOH and in N3/TiO_2/EtOH is significantly red-shifted to 2105 cm^{-1} in N3/TiO_2/ACN. As discussed below, this red-shift may be further evidence for stronger electronic coupling between N3 and TiO_2 in the presence of ACN, as suggested by the red-shift in the absorption spectrum. Both N3-sensitized and bare TiO_2 nanoparticles in ACN consistently showed a large luminescence background at green wavelengths, as can be seen in Figure 7. This luminescence was not observed for nanoparticles in EtOH. We also note that preliminary resonance Raman data (to be published) for N3 adsorbed on a nanocrystalline thin film of TiO_2 do not show any solvent dependence of the ~2105 cm^{-1} band.

Solvent overlap limits the number of N3 Raman bands that can be compared in all three samples. Figures 8, 9, and 10 show Raman excitation profiles (cross section σ_R as a function of excitation wavelength) for the ~700, ~1540, and ~1610 cm^{-1} N3 modes, respectively. The data generally show little difference in σ_R for N3/EtOH compared to N3/TiO_2 in EtOH, and generally higher values for N3/TiO_2 in ACN. The similarity of the Raman

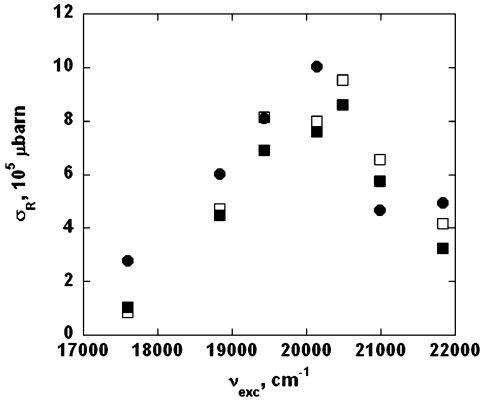

Figure 9. Raman cross section σ_R of the ~1540 cm^{-1} Raman band as a function of excitation frequency for N3 in EtOH (open squares), on TiO_2 in EtOH (filled squares), and on TiO_2 in ACN (filled circles).

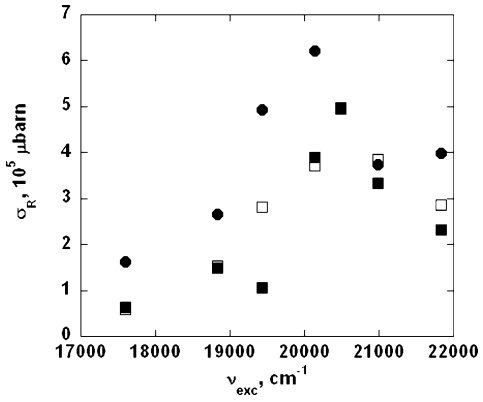

Figure 10. Raman cross section σ_R of the ~1610 cm^{-1} Raman band as a function of excitation frequency for N3 in EtOH (open squares), on colloidal TiO_2 in EtOH (filled squares), and on colloidal TiO_2 in ACN (filled circles).

TABLE 1: Depolarization Ratios ρ of the ~700 cm^{-1} N3 Raman Mode as a Function of Excitation Wavelength

λ_{exc}, nm	N3/EtOH	N3/TiO_2/EtOH	N3/TiO_2/ACN
458	0.73	0.53	
476	0.45	0.49	0.65
488	0.50	0.52	
496	0.44	0.45	0.56
514	0.40	0.39	0.47
530	0.26	0.26	0.28
568	0.31	0.30	0.32

cross sections for free and TiO_2-adsorbed N3 in EtOH is consistent with the similarities in the absorption and emission spectra for these two samples. In all samples, very weak Raman scattering at wavelengths within the blue absorption band at ~400 nm precluded the analysis of Raman cross sections and depolarization ratios at these wavelengths.

Depolarization ratios ρ were determined for the ~700, ~1547, and ~1610 cm^{-1} Raman bands in all three samples and are shown in Tables 1, 2, and 3, respectively. There are definite departures from the values of 1/3 expected for resonance with a single nondegenerate electronic transition, and the dependence of ρ on excitation frequency suggests resonance via more than one excited electronic state. There appears to be a trend for ρ to approach 1/3 at longer wavelengths and increase as the wavelength is tuned toward the blue. The Loppnow group[29] reported ρ values of 0.31, 0.33, and 0.44 for the ~700, ~1547, and 1610 cm^{-1} Raman bands, respectively, with no mention of dispersion. Although it was not possible to determine ρ for a large number of modes in all three samples, the general trend

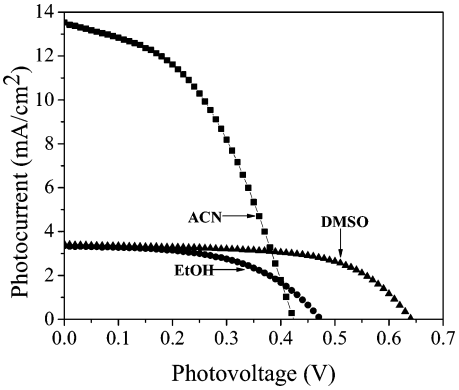

Figure 11. Photocurrent versus photovoltage of N3-sensitized DSSC using ACN, EtOH, and DMSO as the solvent for the electrolyte.

TABLE 2: Depolarization Ratios ρ of the ~1540 cm^{-1} N3 Raman Mode as a Function of Excitation Wavelength

λ_{exc}, nm	N3/EtOH	N3/TiO_2/EtOH	N3/TiO_2/ACN
458	0.49	0.46	0.68
476	0.49	0.52	0.55
488	0.47	0.50	
496	0.45	0.47	0.53
514	0.42	0.45	0.44
530	0.31	0.31	0.36
568	0.34	0.33	0.40

TABLE 3: Depolarization Ratios ρ of the ~1610 cm^{-1} N3 Raman Mode as a Function of Excitation Wavelength

λ_{exc}, nm	N3/EtOH	N3/TiO_2/EtOH	N3/TiO_2/ACN
458	0.67	0.61	0.65
476	0.64	0.67	0.59
488	0.62	0.63	
496	0.58	0.59	0.63
514	0.28	0.57	0.60
530	0.36	0.39	0.44
568	0.47	0.49	0.51

was to observe dispersion in the depolarization ratio and values different from 1/3, as shown in Tables 1−3.

3.3. Dye-Sensitized Solar Cell. Figure 11 shows the photocurrent−photovoltage behavior for a DSSC containing DMSO, EtOH, and ACN as the solvent for the electrolyte. The surface concentration of N3, determined after making the current and voltage measurements, was found to be 1.56×10^{-7} mol/cm^2 for the experiment using ACN, 1.50×10^{-7} mol/cm^2 for EtOH, and 1.66×10^{-7} mol/cm^2 for DMSO. Thus the differences in photocurrent shown in Figure 11 are not merely the result of differences in dye adsorption. The energy conversion efficiency η was determined from

$$\eta = \frac{(IV)_{max}}{P_0} \tag{6}$$

where $(IV)_{max}$ is the maximum value of the product of the photocurrent and the photovoltage, and P_0 is the incident light power. Of the three solvents, ACN gives the largest maximum current I_{sc}, the lowest maximum voltage V_{oc}, and the largest conversion efficiency η. The short-circuit current is similar for DMSO and EtOH, but the enhanced voltage in the former results in greater efficiency in DMSO though it is not as large as that for ACN. The value of η was found to be 2.6% in ACN, 1.3% in DMSO, and 0.84% in EtOH. The solvent trend in the photocurrent is consistent with the previously discussed solvent

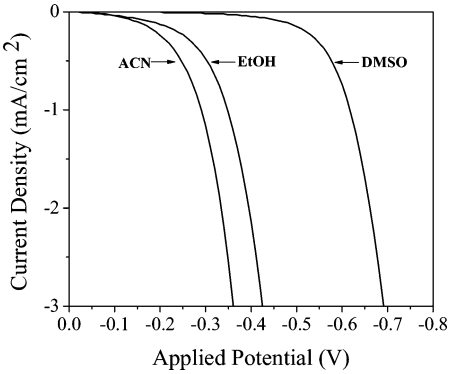

Figure 12. Dark current versus applied voltage of N3-sensitized DSSC using ACN, EtOH, and DMSO as the solvent for the electrolyte.

effects on ϕ_{ET}, though solvent effects on the collection efficiency could also enter into the picture.

The open-circuit voltage is given by[50]

$$V_{oc} = \frac{k_B T}{e} \ln\left(\frac{I_{inj}}{n\sum_i k_i[A_i]}\right) \tag{7}$$

where I_{inj} is the flux of injected electrons, n is the density of electrons in the conduction band, and $k_i[A_i]$ is the rate of recombination of conduction band electrons with acceptor A_i. Equation 7 reveals that for similar electron injection yields the maximum voltage decreases with increasing recombination current, consistent with the solvent trends shown in the current−voltage data of Figures 11 and 12. The smaller short circuit current I_{sc} and larger open circuit voltage V_{oc} found in EtOH and DMSO compared to ACN correlates with a smaller recombination current, and this is indeed confirmed by measurement of the dark current as shown in Figure 12. The dark current at a given applied potential is smallest in magnitude for DMSO and largest for ACN.

4. Discussion

The influence of the solvent on the absorption spectrum of N3 adsorbed on nanoparticulate TiO_2 was found to be very different for amorphous versus crystalline nanoparticles. In the latter, the absorption spectrum of N3 was similar for films in contact with either EtOH or ACN and was red-shifted compared to the dry film. In contrast, the absorption spectrum of N3 on colloidal TiO_2 was red-shifted in ACN compared to EtOH, and there is little difference between the absorption and emission spectra of free versus nanoparticle-adsorbed N3 in EtOH. In addition, we observe the ~400 nm band of N3 on colloidal TiO_2 to be much broader in ACN than in EtOH. This broadening is evidence for coupling to a band of semiconductor states, and such coupling is evidently stronger in ACN than EtOH consistent with faster interfacial ET and greater luminescence quenching in ACN. In addition, the band gap transition of unsensitized TiO_2 was found to be red-shifted in ACN compared to EtOH in the case of the amorphous nanoparticles, whereas it is independent of the contacting solvent in the case of nanocrystalline particles. One might wonder whether quantum effects on the band gap transition could be at work, but these are not expected for particles larger than about 2 nm.[51] A great difference in the kinetic stability to precipitation of colloidal TiO_2 was observed, with suspensions in EtOH being stable for much longer periods of time than those in ACN. Though we cannot completely rule out the possibility that nanoparticle

agglomeration in ACN leads to an apparent red-shift due to enhanced light scattering, the clean baseline in the absorption spectrum of colloidal TiO_2 in ACN argues against this. We conclude that the red-shift of the band gap transition in ACN is more likely to be the result of a surface phenomenon. Surface defects and associated trap states of TiO_2 nanoparticles have been reported to lead to red-shifts in the band gap and the appearance of photoluminescence upon visible excitation, not observed in crystalline TiO_2.[48,52−54] Indeed, luminescence backgrounds were observed in the resonance Raman spectra of N3 on colloidal TiO_2 in ACN, but were not apparent for the EtOH suspensions. In an analogous system, nanoparticles of ZnO synthesized in different solvents were found to have different morphologies and varying amounts of trap state luminescence correlated to the surface-to-volume ratio.[54] Solvent could influence the growth of various crystal planes, or could coordinate to surface defects in the form of dangling bonds. Such surface states are naturally less prevalant in nanocrystalline TiO_2 films which have been subject to sintering at 450 °C.

Hartland et al.,[36] employing mainly amorphous nanoparticles of TiO_2 in ethanol, observed a red-shift in the band gap transition upon addition of water attributed to the interaction of water with surface defects in the form of oxygen vacancies. They also found the electronic coupling between the sensitizer (9-anthracenecarboxylic acid) and the semiconductor to be different for nanoparticles prepared by different synthetic methods and having different degrees of crystallinity. Similarly, the surface states observed here also appear to mediate the electronic coupling between the dye and semiconductor, leading to a red-shift of the N3 absorption band on TiO_2 in ACN relative to EtOH in the case of the amorphous, but not crystalline, nanoparticles. Red-shifts of the absorption spectra of various dyes on TiO_2 relative to free dye are quite prevalent in the literature,[55] and have been speculated to be the result of electronic coupling, image charges, or charge-transfer contributions to the excited state. Indeed large red-shifts in the absorption spectrum of strongly coupled dyes such as alizarin[56] and ascorbic acid[57] are observed and attributed to the formation of dye-surface charge-transfer complexes. These systems represent clear examples of strong electronic coupling resulting from mixing between the dye LUMO and the Ti^{4+} 3d orbitals which comprise the conduction band.[59] It has been pointed out that such strong coupling and resulting ultrafast electron transfer is not ideal for the DSSC because recombination dynamics are also faster.[16] Thus good sensitizers are moderately coupled to the semiconductor and show smaller red-shifts. This electronic coupling influences the rate of electron transfer, and evidence of weak coupling in the case of N3 on colloidal TiO_2 in EtOH, based on the similarity of the absorption spectra of the free and adsorbed dye, is completely consistent with the absence of luminescence quenching of N3 on TiO_2 in this solvent. Despite weak electronic coupling, significant shifts are observed in the Raman spectrum of N3 on adsorption on colloidal TiO_2 in EtOH, consistent with a physical interaction with the surface.

We conclude that N3 is much more strongly coupled to nanocolloidal TiO_2 when it is in contact with ACN compared to EtOH, whereas the electronic coupling in the case of crystalline films appears to be fairly independent of solvent. In the colloidal systems, a solvent effect on this coupling is also evidenced by the red-shift in the vibrational frequency of the C≡N stretch for N3 on TiO_2 in ACN. The SCN^- ligand is not believed to be involved in the binding to the semiconductor, but calculations suggest that the HOMO of N3 is largely localized on this group.[4] The charge-transfer nature of the N3−TiO_2 coupling results in a ground state wave function for the adsorbed dye which contains a small contribution from the oxidized dye. This incipient charge transfer leads to weakening of the C≡N bond and a decrease in vibrational frequency in the more strongly coupled system. In a preliminary resonance Raman study of N3 adsorbed on crystalline TiO_2, we observed this vibrational frequency to be independent of the solvent (ACN or EtOH) in contact with the film, consistent with similar N3 absorption spectra and similar electronic couplings for sensitized nanocrystalline films in contact with ACN and EtOH. This suggests that the coupling in the amorphous particles is between N3 and the surface trap states which are more prevalent in ACN than in EtOH.

For N3-sensitized nanocrystalline ZrO_2 films in contact with solvent, the luminescence intensity is largest in DMSO and smallest in ACN, reflecting differences in the rate of nonradiative relaxation via energy transfer to solvent. In each solvent, the emission intensity is largely quenched for N3 on nanocrystalline TiO_2 compared to ZrO_2, with the largest quenching ($\phi_{ET} \approx 0.98$) observed for ACN. This is consistent with faster interfacial ET and larger photocurrent for the DSSC employing ACN compared to EtOH and DMSO. The maximum (short-circuit) photocurrent I_{sc} reflects the quantum yield of interfacial ET, the light-harvesting efficiency, and the collection efficiency for injected electrons. The absorption spectrum of N3 adsorbed on nanocrystalline TiO_2 is not very solvent dependent, and the differences in dye-loading for films in contact with different solvents were minor, so we may neglect solvent effects on the light-harvesting efficiency. DSSCs containing EtOH and DMSO were found to have similar I_{sc} even though slightly larger ϕ_{ET} is observed for EtOH compared to DMSO, reflecting decreased collection efficiency in the presence of EtOH relative to DMSO. Increased photocurrent also correlates with smaller maximum voltage V_{oc} and increased dark current, as it is well-known that the maximum photovoltage is limited by recombination of conduction band electrons with oxidized species.[50] Thus the solvent trends in the photocurrent, dark current, and luminescence are all consistent with the rate of interfacial ET that increases in the series DMSO < EtOH < ACN. Though the ultrafast component of interfacial ET from N3 to nanocrystalline TiO_2 has been found to be independent of solvent, the luminescence spectra used to determine ϕ_{ET} reveal the slower time scale injection processes as well. If the overall rate k_{et} of eq 5 were independent of solvent as well, then the slower nonradiative relaxation in DMSO would have resulted in a higher quantum efficiency, in contrast to our observations. Thus we conclude that the total rate of electron injection (not just the subpicosecond component) is largest for ACN and smallest for DMSO.

The crystallinity of the nanoparticles is an important factor in promoting interfacial ET, and the superior performance of the anatase crystalline form compared to rutile in the DSSC is well-known. It is reasonable to consider that solvent effects on the conduction band edge could alter the rate of interfacial ET as well as that of back-electron transfer. The driving force for interfacial ET is given by

$$\Delta G^\circ = E^\circ(D^*/D^+) - E_{CB}(TiO_2) \qquad (8)$$

where $E^\circ(D^*/D^+)$ is the reduction potential energy of the dye in its excited electronic state, and $E_{CB}(TiO_2)$ is the potential energy of the conduction band edge. The flat band potential of nanoparticulate TiO_2 films has been found to be solvent dependent. Fitzmaurice et al.[24] determined E_{CB} by measuring the absorbance of the conduction band electrons in TiO_2

nanocrystalline films in contact with various solvents as a function of applied potential. In the absence of Li^+, they found that the flat band potentials (versus SCE) were -2.04 V for films in contact with ACN, shifting to a more positive potential of -1.39 V in contact with EtOH, for solutions containing 0.2 M tetrabutylammonium perchlorate. The value of $E_{CB}(TiO_2)$ was reported to be sensitive to added Li^+ ion, which lowers the conduction band and has a larger effect for films in contact with ACN than in EtOH. For the 0.5 M Li^+ concentrations used in the present study, the data of ref 24 suggest that the conduction band in the case of ACN could actually be somewhat lower (less negative) than for EtOH. All other factors being equal, this would result in a greater driving force and faster ET in the case of ACN. Following Marcus theory,[58] the activation barrier for ET depends on this driving force as well as the solvent and internal reorganization energies. For the normal Marcus regime relevant to forward ET, increasing reorganization energy would result in a larger barrier and slower rate of ET. It is interesting that the highest yield of interfacial ET is found when the sensitized film is in contact with a solvent in which the free dye is not soluble. EtOH and DMSO would be expected to interact more strongly with the adsorbed dye, since the free dye is soluble in both these solvents, perhaps resulting in larger solvent reorganization energy and a larger barrier to ET.

The observed photocurrent also depends on the rate of back-electron transfer, assumed to be dominated by recombination of conduction band electrons with I_3^-.[63−65] This recombination has been reported to take place in the Marcus inverted regime where k_{ET} decreases with increasing driving force, which is given by the difference in E_{CB} and the reduction potential energy of the I^-/I_3^- redox couple. The standard reduction potential for the conversion of I_3^- to I^- shifts from 0.48 V in DMSO (versus SCE) to 0.40 V in methanol, to 0.25 V in ACN.[21,25] Assuming that the value in EtOH is similar to that in methanol and neglecting solvent effects on E_{CB}, the driving force for recombination should be largest for DMSO and smallest for ACN based on the position of the I_3^-/I^- redox potential. These values are consistent with the observed trends in recombination current which decreases in magnitude on going from ACN to EtOH to DMSO.

Though great care was taken to employ dry solvents in the present work, water is known to be strongly adsorbed on the surface of TiO_2 and may play a role in the ultrafast ET from adsorbed sensitizers.[60,61] N3 as received contains two waters of hydration, and the possible formation of an ester linkage by reaction of its carboxylic acid groups with surface hydroxyls on TiO_2 would produce more water which would presumably be adsorbed on the surface. Preferential adsorption of water from mixed water/ACN solution onto nanocrystalline TiO_2 was reported in ref 62. The presence of a water layer along with Li^+ ions adsorbed at the photoanode could level out the expected influence of the bulk organic solvent on the conduction band; nevertheless, strong solvent effects on the quantum yield ϕ_{ET}, the photocurrent, and the photovoltage are observed. In the amorphous particles, the solvent has an apparently strong influence on the surface trap states. We suggest that such solvent effects may also operate to modify the surface structure in the case of nanocrystalline films as well, thereby influencing interfacial ET and recombination dynamics.

The fastest component of interfacial ET from N3 to TiO_2, previously reported to be independent of solvent, might have been expected to lead to lower Raman cross sections for adsorbed N3 in both ACN and EtOH. However, the absence of quenching of the N3 luminescence on adsorption on colloidal TiO_2 in EtOH argues that the rate of interfacial ET is much slower than for N3 on TiO_2 in ACN. We find little change in the Raman intensity on adsorption for samples in EtOH, and generally greater intensity in the case of N3 on TiO_2 in ACN. As previously mentioned, part of this difference could be the result of larger solvent reorganization in EtOH than ACN, consistent with negligible solubility of N3 in the latter solvent. In addition, it is suggested that increased electronic coupling of the sensitizer and semiconductor in ACN, evidenced by the large red-shift in the absorption spectrum on colloidal TiO_2 in ACN versus EtOH, could play a role, as this would correlate with a larger overall rate of ET. We speculate that such coupling could provide a mechanism for intensity borrowing from the very strong band gap transition of TiO_2. This hypothesis will be explored in future work by examining resonance Raman spectra of sensitizer/semiconductor systems with a range of electronic couplings and by examining resonance Raman spectra of sensitizers on nanocrystalline films.

The observed dispersion in the resonance Raman depolarization ratios found here is consistent with resonance enhancement via more than one electronic state. However, the mirror-image relationship between the luminescence spectrum and the ~530 nm absorption band of N3 (see for example Figure 2 of ref 5) argues against the conclusion that this band is a composite of many electronic transitions, as suggested by the calculations.[31,32] Consistent with this, it was found here that the depolarization ratios of N3 Raman bands tend to approach 1/3 as the wavelength is tuned to the red. Weak resonance Raman signals for N3 spectra excited within the blue absorption band at about 400 nm as well as the results of ref 33, on the other hand, *might* be due to the existence of multiple electronic transitions within this band. However, it is well-known that interference of two resonant electronic states can lead to enhancement or cancellation of Raman intensity at excitation energies intermediate between the transitions.[66] Thus we cannot rule out the possibility of interference effects from the putative MLCT and ligand-based transitions which could lead to a reduction in Raman intensity at blue wavelengths.

5. Conclusions

The effect of solvent on the efficiency of interfacial electron transfer has been explored in colloidal and crystalline nanoparticles of TiO_2 sensitized by N3 dye. In the colloidal particles, interfacial ET is observed for sensitized particles in acetonitrile but not in ethanol. Resonance Raman and absorption spectra suggest much stronger coupling, mediated by surface states, between N3 and TiO_2 for the colloidal particles in ACN as compared to EtOH. In contrast, interfacial ET from N3 to nanocrystalline TiO_2 takes place for films in contact with ACN, EtOH, and DMSO with quantum efficiency ranging from about 0.8 in DMSO to near unity in ACN, consistent with the rate of electron injection which is largest in ACN and smallest in DMSO. Higher photocurrents and smaller open-circuit photovoltages are observed for dye-sensitized solar cells using ACN as compared to EtOH or DMSO as the solvent for the redox couple and are consistent with recombination currents which increase on going from DMSO to EtOH to ACN. The solvent series examined here highlights the tradeoff in optimizing the efficiency of solar energy conversion, in that higher photocurrents are accompanied by lower photovoltages owing to factors which simultaneously favor forward and reverse electron transfer. Future work will examine the possible effect of solvent on the morphology and transport properties of nanocrystalline films of TiO_2 and explore whether the solvent effects reported here are tied to surface properties of the semiconductor.

Acknowledgment. Support from the National Science Foundation through Grant CHE 0202784 and from the Washington State University College of Science and Department of Chemistry is gratefully acknowledged. We thank Ms. Suzanne Lanier for contributions to the measurement of solar conversion efficiencies.

References and Notes

(1) O'Regan, B. Grätzel, M. *Nature* **1991**, *353*, 737.
(2) Grätzel, M. *Nature* **2001**, *414*, 338.
(3) Hagfeldt, A.; Grätzel, M. *Acc. Chem. Res.* **2000**, *33*, 269.
(4) Hagfeldt, A.; Grätzel, M. *Chem. Rev.* **1995**, *95*, 49.
(5) Nazeeruddin, M. K.; Kay, A.; Rodicio, I.; Humphry-Baker, R. Müller, E.; Liska, P.; Vlachopoulos, N.; Grätzel, M. *J. Am. Chem. Soc.* **1993**, *115*, 6382.
(6) Benkö, G.; Kallioinen, J.; Korppi-Tommola, J. E. I.; Yartsev, A. P.; Sundstrom, V. *J. Am. Chem. Soc.* **2002**, *124*, 489.
(7) Benkö, G.; Kallioinen, J.; Myllyrperkiö, P.; Trif, F.; Korppi-Tommola, J. E. I.; Yartsev, A. P.; Sundström, V. *J. Phys. Chem. B* **2004**, *108*, 2862.
(8) Kallioinen, J.; Benkö, G.; Sundström, V.; Korppo-Tommola, J. E. I.; Yartsev, A. P. *J. Phys. Chem. B* **2002**, *106*, 4396.
(9) Asbury, J. B.; Ellingson, R. J.; Ghosh, H. N.; Ferrere, S.; Nozik, A. J. Lian, T. *J. Phys. Chem. B* **1999**, *103*, 3110.
(10) Asbury, J. B.; Hao, E.; Wang, Y.; Ghosh, H. N.; Lian, T. *J. Phys. Chem. B* **2001**, *105*, 4545.
(11) Lenzmann, F.; Kruegar, J.; Burnside, S.; Brooks, K.; Grätzel, M.; Gal, D.; Rühle, S.; Cahen, D. *J. Phys. Chem. B* **2001**, *105*, 6347.
(12) Kuciauskas, D.; Freund, M. S.; Gray, H. B.; Winkler, J. R.; Lewis, N. S. *J. Phys. Chem. B* **2001**, *105*, 392.
(13) Kuciauskas, D.; Monat, J. E.; Villahermosa, R.; Gray, H. B.; Lewis, N. S.; McCusker, J. K. *J. Phys. Chem. B* **2002**, *106*, 9347.
(14) Wenger, B.; Grätzel, M.; Moser, J.-E. *Chimia* **2005**, *59*, 123.
(15) Durrant, J. R.; Tachibana, Y.; Mercer, I.; Moser, J. E.; Grätzel, M.; Klug, D. R. *Z. Phys. Chem.* **1999**, *212*, 93.
(16) Durrant, J. R.; Haque, S. A.; Palomares, E. *Coord. Chem. Rev.* **2004**, *248*, 1247.
(17) Kalyanasundaraman, K.; Grätzel, M. *Coord. Chem. Rev.* **1998**, *177*, 347.
(18) Watson, D. J.; Meyer, G. J. *Coord. Chem. Rev.* **2004**, *248*, 1391.
(19) Gregg, B. A.; Chen, S.-G.; Ferrere, S. *J. Phys. Chem. B* **2003**, *107*, 3019.
(20) Li, Y.; Hagen, J.; Schaffrath, W.; Otschik, P.; Haarer, D. *Sol. Energy Mater. Sol. Cells* **1999**, *56*, 167.
(21) Mann, C. K.; Barnes, K. K. *Electrochemical Reactions in Nonaqueous Solvents*; Marcel Dekker: New York, 1970.
(22) Argazzi, R.; Bignozzi, C. A.; Yang, M.; Hasselmann, G. M.; Meyer, G. J. *Nano Lett.* **2002**, *2*, 625.
(23) Waterland, M. R.; Kelley, D. F. *J. Phys. Chem. A* **2001**, *105*, 4019.
(24) Redmond, G.; Fitzmaurice, D. *J. Phys. Chem.* **1993**, *97*, 1426.
(25) Iwamoto, R. T. *Anal. Chem.* **1959**, *31*, 955.
(26) McHale, J. L. *Acc. Chem. Res.* **2001**, *34*, 265.
(27) Myers, A. B. *Acc. Chem. Res.* **1997**, *30*, 519.
(28) Lee, S.-Y.; Heller, E. J. *J. Chem. Phys.* **1979**, *71*, 4777.
(29) Shoute, L. C. T.; Loppnow, G. R. *J. Am. Chem. Soc.* **2003**, *125*, 15636.
(30) Guillemoles, J.-F.; Barone, V.; Joubert, L., Adamo, C. *J. Phys. Chem. A* **2002**, *106*, 11354.
(31) Fantacci, S.; De Angelis, F.; Selloni, A. *J. Am. Chem. Soc.* **2003**, *125*, 4381.
(32) Monat, J. E.;. Rodriguez, J. H.; McCusker, J. K. *J. Phys. Chem. A* **2002**, *106*, 7399.
(33) Bhasikuttan, A. C.; Okada, T. *J. Phys. Chem. B* **2004**, *108*, 12629.
(34) Hao, E.; Anderson, N. A.; Asbury, J. B.; Lian, T. *J. Phys. Chem. B* **2002**, *106*, 10191.
(35) Schlictörl, G.; Huang, S. Y.; Sprague, J. Frank, A. J. *J. Phys. Chem. B* **1997**, *101*, 2529.
(36) Martini, I.; Hodak, J. H.; Hartland, G. V. *J. Phys. Chem. B* **1998**, *102*, 607.
(37) Wang, H.; He, J.; Boschloo, G.; Lindström, H.; Hagfeldt, A.; Lindquist, S.-E. *J. Phys. Chem. B* **2001**, *105*, 2529.
(38) Stergiopoulos, T.; Bernard, M.-C.; Hugot-le Goff, A.; Falares, P. *Coord. Chem. Rev.* **2004**, *248*, 435−461.
(39) Greijer, H.; Lindgren, J.; Hagfeldt, A. *J. Phys. Chem. B* **2001**, *105*, 6314.
(40) Kormann, C.; Bahnemann, D. W.; Hoffmann, M. R. *J. Phys. Chem.* **1988**, *92*, 5196.
(41) Baddour-Hudjean, R.; Bach, S.; Smirnov, M.; Pereira-Ramos, J.-P. *J. Raman Spectrosc.* **2004**, *35*, 577.
(42) Chang, H.; Huang, P. J. *J. Raman Spectrosc.* **1998**, *29*, 97.
(43) Pottier, A.; Cassaignon, S.; Chanéac, C.; Villain, F.; Tronc, E.; Jolivet, J.-P. *J. Mater. Chem.* **2003**, *13*, 877.
(44) Zong, Y.; McHale, J. L. *J. Chem. Phys.* **2004**, *120*, 11333.
(45) Zhao, X.; Burt, J. A.; McHale, J. L. *J. Chem. Phys.* **2004**, *121*, 11195.
(46) Smestad, G. P.; Grätzel, M. *J. Chem. Educ.* **1998**, *75*, 752.
(47) Nazeeruddin, Md. K.; Zakeeruddin, S. M.; Humphrey-Baker, R.; Jirousek, M.; Liska, P.; Vlachopoulos, N.; Shklover, V.; Fischer, V.; Grätzel, M. *Inorg. Chem.* **1999**, *38*, 6298.
(48) Nelson, J. *The Physics of Solar Cells*; Imperial College Press: London, 2003.
(49) Tachibana, Y.; Moser, J. E.; Grätzel, M.;, Klug, D. R.; Durrant, J. R. *J. Phys. Chem.* **1996**, *100*, 20056.
(50) Meyer, G. J. *J. Photochem. Photobiol. A* **2003**, *158*, 119. 4
(51) Serpone, N.; Lawless, D.; Khairutdinov, R. *J. Phys. Chem.* **1995**, *99*, 16646.
(52) Zhang, W. F.; Zhang, M. S.; Yin, Z.; Chen, Q. *Appl. Phys. B* **2000**, *70*, 261.
(53) Zhu, Y. C.; Ding, C. X. *J. Solid State Chem.* **1999**, *145*, 711.
(54) Andelman, T.; Gong, Y.; Polking, M.; Yin, M.; Kuskovsky, I.; Neumark, G.; O'Brien, S. *J. Phys. Chem. B* **2005**, *109*. 14314.
(55) Pant, D.; Levinger, N. *J. Phys. Chem. B* **1999**, *103*, 7846.
(56) Shoute, L. C.; Loppnow, G. R. *J. Chem. Phys.* **2002**, *117*, 842.
(57) Xagas, A. P.; Bernard, M. C.; Hugot-Le Goff, A.; Spyrellis, N.; Loizos, Z.; Falaras, P. *J. Photochem. Photobiol. A* **2000**, *132*, 115.
(58) Gao, Y.; Marcus, R. A. *J. Chem. Phys.* **2000**, *113*, 6351.
(59) Mulliken, R. S.; Person, W. B. *Molecular Complexes*; Wiley-Interscience: New York, 1969.
(60) Onda, K.; Li, B,; Zhao, J.; Jordan, K. D.; Yang, J.; Petek, H. *Science* **2005**, *308*, 1154.
(61) Lian, T. Personal communication.
(62) Enright, B.; Redmond, G.; Fitzmaurice, D. *J. Phys. Chem.* **1994**, *98*, 6195.
(63) Sauvé, G.; Cass, M. E.; Coia, G.; Doig, S. J.; Lauermann, I.; Pomykal, K. E.; Lewis, N. S. *J. Phys. Chem. B* **2000**, *104*, 6821.
(64) Frank, A. J.; Kopidakis, N.; van de Lagemaat, J. *Coord. Chem. Rev.* **2004**, *248*, 1165.
(65) Fabregat-Santiago, F.; Garcia-Belmonte, G.; Boschloo, G.; Hagfeldt, A. *Sol. Energy Mater. Sol. Cells* **2005**, *87*, 117.
(66) Bailey, S. E.; Cohan, J. S.; Zink, J. I. *J. Phys. Chem. B* **2000**, *104*, 10743.